Effect of gas composition on temperature and CO_2 conversion in a gliding arc plasmatron reactor : insights for post-plasma catalysis from experiments and computation

RESEARCH ARTICLE

Effect of Gas Composition on Temperature and CO_2 Conversion in a Gliding Arc Plasmatron reactor: Insights for Post-plasma Catalysis from Experiments and Computation

Wencong Xu,[a,b,c,1] Senne Van Alphen, [b,1] Vladimir V. Galvita,[c] Vera Meynen,[a] and Annemie Bogaerts *[b]

[a] Wencong Xu, Prof. Vera Meynen
Department of Chemistry, Research group LADCA
University of Antwerp
Universiteitsplein 1, B-2610 Wilrijk, Antwerp, Belgium

[b] Senne Van Alphen, Prof. Annemie Bogaerts
Department of Chemistry, Research group PLASMANT
University of Antwerp
Universiteitsplein 1, B-2610 Wilrijk, Antwerp, Belgium
*corresponding author: E-mail: annemie.bogaerts@uantwerpen.be

[c] Prof. Vladimir V. Galvita
Department of Materials, Textiles and Chemical Engineering, Research group LCT
Ghent University
Technologiepark 125, B-9052, Ghent, Belgium

[1] The authors equally contributed to this work

Abstract: Plasma-based CO_2 conversion has attracted increasing interest. However, to understand the impact of plasma operation on post-plasma processes, we studied the effect of adding N_2, N_2/CH_4 and $N_2/CH_4/H_2O$ to a CO_2 gliding arc plasmatron (GAP) to obtain valuable insights into their impact on exhaust stream composition and temperature, which will serve as feed gas and heat for post-plasma catalysis (PPC). Adding N_2 improves the CO_2 conversion from 4% to 13%, and CH_4 addition further promotes it to 44%, and even to 61% at lower gas flow rate (6 L/min), allowing a higher yield of CO and hydrogen for PPC. The addition of H_2O, however, reduces the CO_2 conversion from 55% to 22%, but it also lowers the energy cost, from 5.8 to 3 kJ/L. Regarding the temperature at 4.9 cm post-plasma, N_2 addition increases the temperature, while the CO_2/CH_4 ratio has no significant effect on temperature. We also calculated the temperature distribution with computational fluid dynamics simulations. The obtained temperature profiles (both experimental and calculated) show a decreasing trend with distance to the exhaust and provide insights in where to position a PPC bed.

Introduction

In the past decades, accumulating evidence has demonstrated that the increasing emission of greenhouse gases is leading to global warming.[1] Specifically, the concentration of CO_2 in the atmosphere has risen significantly, surging from 362 ppm at the end of the last century to 420 ppm in June 2023, based on the data from the "National Oceanic and Atmospheric Administration (NOAA) Global Monitoring Laboratory".[2] Therefore, numerous techniques are being developed to capture CO_2 and convert it into value-added fuels or chemical products.[3–7] Several different chemical processes, including CO_2 splitting (Eq.(1)), CO_2 methanation with H_2 (Eq.(2)), and CO_2 dry reforming of methane (DRM) Eq.(3), have been investigated for the conversion of CO_2 either directly or in combination with other molecules like CH_4, H_2, or/and H_2O.[8–10] However, as a relatively stable molecule, the activation of CO_2 remains a significant challenge for many (catalytic) reactions. Thermally, direct CO_2 splitting is energy-consuming and only favorable at high temperature. For instance, at 2000 K, it is estimated that, to achieve a CO_2 conversion of 1.5%, the energy cost (EC) will be about 7.9 MJ/mol and the final energy efficiency (EE) is just 4.4%.[11]

$$CO_2 \rightarrow CO + 1/2\, O_2, \Delta H^0 = 280\, kJ/mol \quad (1)$$

$$CO_2 + 4H_2 \rightarrow CH_4 + 2H_2O, \Delta H^0 = -165\, kJ/mol \quad (2)$$

$$CO_2 + CH_4 \rightarrow 2CO + 2H_2, \Delta H^0 = 247\, kJ/mol \quad (3)$$

In recent years, plasma technology has been widely applied in CO_2 conversion because it can activate the gas molecules by electron impact excitation, ionization and dissociation via electrical energy supply. This creates excited species, ions and radicals that can form new molecules.[11,12] Compared with conventional thermal approaches, electrical energy is transferred to the gas, making it a promising technology for the ongoing energy transition in chemical production.[13–18] Furthermore, plasma can be integrated with catalysts to create a hybrid plasma-catalysis process, which holds promise for enhancing CO_2 conversion, improving energy efficiency and chemical product selectivity.[15,19–21] A lot of research on CO_2 conversion is performed with various kinds of plasmas, including a dielectric barrier discharge (DBD),[22] microwave (MW),[23] spark or gliding arc (GA) discharge.[12,24] Among these plasma techniques, gliding arc plasma is promising, because it can typically produce electrons with mean energy around 1 eV, which is ideal to activate

CO_2.[12,25] Moreover, the GA creates heat in the plasma zone, with temperatures up to a few 1000 K,[26,27] which influences the reactions and allows for post-plasma catalysis in the exhaust stream of the plasma reactor, recovering (at least part of) the heat of the plasma process.[14,28]

Several different types of GA plasmas have been designed, e.g. classical 2D GA,[29] 3D rotating gliding arc (RGA),[30,31] 3D gliding arc plasmatron (GAP),[12] and dual-vortex plasmatron (DVP).[27] The classical 2D GA plasma is widely studied, however, it exhibits some drawbacks, as it is incompatible with industrial application because of its 2D flat electrodes. Furthermore, not all the gas passes through the arc, and thus it is not fully activated. Finally, a relatively high gas flow rate is needed to sustain the arc gliding process, which gives rise to a short gas residence time in the plasma. To overcome these problems, several 3D gliding arc plasma reactor designs have been developed over the years, in which the gas flows tangentially into the reactor, forming a stable vortex gas flow.[12,30,32] Furthermore, recently, a novel DVP reactor was designed and tested, enabling to separate the arc into two directions with longer residence time and highly turbulent flow.[27] These 3D GA reactors are also characterized by high flow rates, but the mechanism to sustain the arc gliding mechanism is different from 2D GA reactors, with typically a cylindrical arc column along the reactor axis, giving rise to a longer gas residence time in the plasma.

Ramakers et al. studied the conversion of CO_2 in the GAP reactor, yielding as highest CO_2 conversion 8.6% and an energy efficiency EE of 30% at an energy cost EC of 39 kJ/L.[12] The group PLASMANT also investigated DRM in the GAP, achieving absolute CO_2 and CH_4 conversions of about 24% and 42%, or effective conversions of about 18% and 10%, respectively, at a CH_4 fraction of 25% in the gas flow, corresponding to an EC of 10 kJ/L and an EE of 66%.[24] In a later study, the same group reported DRM upon addition of N_2 and O_2 in the same GAP reactor, and obtained absolute CO_2 conversions between 31% and 52%, and CH_4 conversions between 55 and 99%, corresponding to a total EC of 13 – 20 kJ/L (or 3.4 - 5.0 eV/molec), depending on the gas mixture.[33] Recently, the addition of only N_2 on the DRM process was studied, and it was found that 20% N_2 addition yields CO_2 and CH_4 absolute conversions of 29 and 36%. However, these values rise notably upon N_2 addition, up to 48% for CO_2 and 61% for CH_4 at 80% N_2.[34]

To fully make use of the heat produced by the GA plasma, research has been focused on establishing synergistic effects of heterogeneous catalysis in combination with the plasma. Zhang et al. reported a combination of a GA plasma with a post-plasma TiO_2 bed for CO_2 splitting.[35] Simulation of the addition of the post-plasma catalyst bed indicated that a strong backflow was formed and experiments confirmed an enhancement in reaction performance. Notably, when the distance between the plasma reactor outlet and the catalyst bed was only 5 mm, fluctuations in CO_2 conversion and EE occurred at flow rates lower than 4 L/min. A synergistic effect was observed because the presence of TiO_2 enhanced the CO_2 conversion from 4.6 to 10.8% and the EE from 5.4 to 12.6% at a gas flow rate of 2 L/min. In another study, 25% increase of CH_4 conversion, 20% increase of CO_2 conversion, around 30% increase in H_2 yield and about 22% increase in EE were achieved when combining a NiO/Al_2O_3 catalyst post-plasma with a GA plasma in DRM.[36] Significant improvements were obtained when a GA plasma was combined with a $Ni/CeO_2/Al_2O_3$ catalyst post-plasma and extra heating was supplied to the catalyst by a tubular furnace.[37] When there was no extra heating, the performance of the plasma with catalyst was almost the same as the plasma alone. This could be explained because of the low temperature (around 300-500 °C) of the plasma gas effluent, at which range the catalyst was inactive for DRM. When the tubular furnace was heated, the combined effect of plasma and catalyst resulted in an increase in CO_2 and CH_4 conversion, from about 25% and 39% in plasma alone, and 62% and 46% in thermal catalysis, to 70% and 59% in the case of plasma catalysis with heating, respectively. Hence, the temperature at the outlet of the plasma GAP reactor is important when combining it with a post-plasma catalytic bed. Nevertheless, to our knowledge, little literature reported on the variation of temperature after plasma in relation to the gas composition used.

In this paper, we employed a GAP setup, which was reported before,[38] to investigate the impact of additives such as N_2, CH_4, and H_2O vapor on the CO_2 conversion. We aim to provide suggestions for selecting optimal conditions for enhanced CO_2 conversion. Moreover, we recorded the temperature after the plasma, offering insights in where to position the catalyst in a post-plasma catalysis (PPC) system. Additionally, we performed simulations to analyze the temperature distribution within the GAP reactor and post-plasma reactor tube, providing a potential view for designing post-plasma catalysis systems.

Results and Discussion

CO_2 and CH_4 conversion

To quantify the CO_2 and CH_4 conversions, the absolute and effective conversions of these two gases were defined. The absolute conversion (Figure 1, solid lines), or simply called “conversion”, gives a direct comparison between the different configurations, while the effective conversion (Figure 1, dash lines) considers the dilution of CO_2 or CO_2/CH_4 in N_2, which is relevant for application and economics as this dilutes and thus limits the products formed.

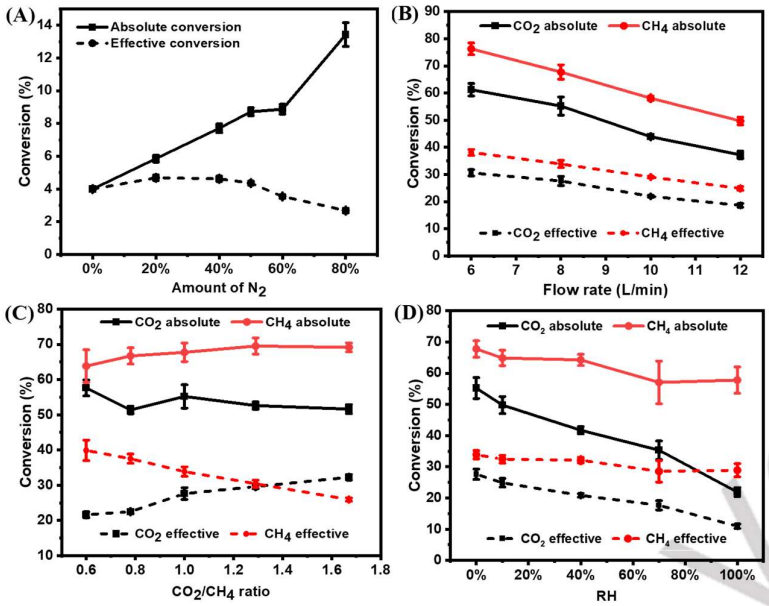

Figure 1. Conversion of CO_2 and CH_4 as a function of gas composition, gas flow rate and relative humidity (RH). (A) CO_2 conversion in CO_2/N_2 mixture: Total gas flow rate = 10 L/min, N_2 fraction varying from 0% to 80%. (B-D) CO_2 and CH_4 conversion in $CO_2/CH_4/N_2$ mixture (B,C), and with H_2O addition (D): (B) Total gas flow rate varied from 6 to 12 L/min, $CO_2/CH_4/N_2$ = 1/1/8. (C) Total gas flow rate = 8 L/min, N_2 = 6.4 L/min, CO_2/CH_4 ratio varied between 0.6 and 1.67. (D) Total gas flow rate = 8 L/min, $CO_2/CH_4/N_2$ = 1/1/8, H_2O amount varied between 0% and 100% RH.

Figure 1 presents the conversions of CO_2 and CH_4 in different gas mixtures. In the CO_2/N_2 gas composition, a significant increase in absolute conversion of CO_2 is observed when N_2 was added into CO_2 from 0% to 80%, as shown in Figure 1A. The value especially increases significantly when the N_2 fraction rises from 60% to 80%. A maximum absolute conversion of 13% was obtained for a N_2 fraction of 80%. Therefore, N_2 in the feed gas is beneficial for converting CO_2. The reason for this was explained already in literature: the CO_2 conversion in a GAP is most effective through the vibrational levels and the high N_2 vibrational levels help to populate the CO_2 vibrational levels.[38] It is interesting to note that at N_2 fractions of 50% and 60%, the CO_2 absolute conversion remained almost the same. This trend is similar as the trend in temperature (Figure 6A) at N_2 fraction of 50% and 60%. On the one hand, N_2 is contributing to the CO_2 conversion, by collisions between vibrationally or electronically excited levels of N_2, which help in the dissociation of CO_2, but the effect of course becomes relatively less pronounced at higher N_2 fractions. On the other hand, the CO_2 conversion also rises upon higher temperature, as the conversion proceeds mainly by thermal chemistry, and because the temperature does not increase in this range (cf. Figure 6A), the CO_2 conversion also stays constant. Moreover, at N_2 fractions above 60%, the CO_2 conversion increased much more. The temperature data, as shown in Figure 6A, shows a similar trend. It seems that the N_2 promotion effect at fractions below 50% is weaker than at fractions above 60%. For the fraction between 50% and 60%, a combined effect results in the CO_2 conversion and gas temperature remaining almost the same, which is probably because the energy transfer from N_2, which increases the gas temperature (the mechanism for it is explained in the followed temperature part), compensates the energy needed for the rise in CO_2 conversion.

For the effective conversion of CO_2, however, because of the decreasing CO_2 fraction in the mixture, the effective conversion of CO_2 shows the opposite trend, with first a slight increase from 4% to 4.7% up to 20% N_2 fraction, and then a drop to 2.7% with increasing N_2 fraction. As the N_2 fraction is lower than 50%, the increase in absolute CO_2 conversion can, to some extent, compensate for the lower concentration of CO_2, but with a higher N_2 fraction, the rise in conversion is not enough to compensate for the drop in CO_2 conversion.[38]

At the same gas flow rate of 10 L/min, once CH_4 is added into the mixture (Figure 1B), the absolute conversion of CO_2 increases to 43%, more than three times the maximum value in the CO_2/N_2 mixture. Moreover, the conversion of CO_2 increases upon decreasing gas flow rate, reaching its highest value of 61% at a flow rate of 6 L/min. The reason that the highest conversion is obtained at the lowest flow rate is due to the longer residence time, giving sufficient time for more gas molecules to react in the plasma region. It should be noticed that when the gas flow rate was increased from 6 L/min to 12 L/min, the pressure of the inlet gas also increased a bit, as measured by the pressure gauge, shown in the Supporting Information; see experimental section, Figure S1. Furthermore, at higher flow rates (e.g., 14 L/min), plasma ignition was very difficult, and the plasma arc became unstable. Besides this, the conversion of CH_4 is always higher than that of CO_2 because the energy needed for the plasma-based decomposition of CH_4 is lower than that for CO_2, due to the lower bond strength to break the C-H vs C=O bond (i.e., 4.48 eV vs 5.52 eV).[33] Since the ratio of CO_2/CH_4 did not change in Figure 1B, the effective conversions of both CO_2 and CH_4 show the same trend as the absolute conversions, but the values are obviously lower. As shown in Figure 2B, although a higher CO_2 conversion was obtained at lower flow rates, the cathode can be seriously damaged. Therefore, we used a gas flow rate of 8 L/min, at which the cathode was safe, to study how the CO_2/CH_4 ratio affects the conversion results.

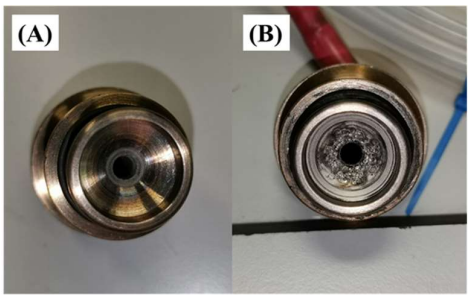

Figure 2. Photographs of (A) clean reactor cathode, and (B) after reaction with a gas flow rate of 6 L/min, indicating clear damage of the cathode.

Figure 1C illustrates that a higher CO_2/CH_4 ratio slightly increases the absolute conversion of CH_4 from 64% to 69%, while the conversion of CO_2 first decreases a bit from about 58% (CO_2/CH_4 ratio of 0.6) to 51% (CO_2/CH_4 ratio of 0.78) and then stays generally constant. However, different from the absolute conversion, the effective conversion of CH_4 decreases significantly from 40% to 26% as the CO_2 fraction increases, while the CO_2 effective conversion shows an obvious increase from 22% to 32%. These conversion values are in line with previous results obtained for the GAP in $CO_2/CH_4/N_2$ mixtures,[34] but they give additional insights into how to adjust the CO_2/CH_4 ratio for achieving better results.

For the PPC system, the outlet gas of the plasma will be utilized as the feed gas for the catalyst to further convert the unreacted reactants or the products from the plasma. This catalyst is a thermal catalyst, which will possibly suffer from deactivation due to coke deposition. Addition of H_2O can help to decrease the formation of solid carbon, as well as produce more H_2.[39] Therefore, we also added H_2O into the feed gas. Compared with DRM without water, adding water causes a serious drop in the absolute conversion of CO_2, from 55% to 22% for a RH ranging from 0% to 100% (Figure 1D). This is attributed to the drop in electron density, as water is trapping the electrons.[39] Another reason is probably that the OH radicals produced by water splitting react with CO, forming CO_2 again, as revealed by detailed chemical kinetics modeling for DBD plasma, where a similar effect was observed.[40] The CH_4 conversion decreases less, from 68% to 58%. The effective conversions of CO_2 and CH_4 show the same, but less significant decreasing tendency. This is different from literature, where it was reported that the CH_4 conversion increases as the molar ratio of H_2O molecules to carbon atoms increases from 0 to 0.58.[39] This may be due to the difference in CO_2/CH_4 ratio. They used a 1.5 times higher ratio than what we used (ratio of 1).

Products selectivity and H_2/CO ratio

As is clear from Figure 3A, the selectivities of CO and H_2 both increase slightly upon increasing gas flow rate, from 68% to 75%, and from 80% to 85%, respectively. In contrast, the selectivity of C_2H_2 first drops from 22 to 18%, and then remains constant around 19% upon higher gas flow rates. The H_2/CO ratio shows a similar trend, as it decreases firstly from 1.6 to 1.5 and then remains constant at a ratio of 1.4.

As the CO_2/CH_4 ratio increases from 0.6 to 1.67, the selectivity of CO keeps increasing from 45% to 93%, while the selectivity of H_2 remains at a high level above 81% and fluctuates around 90%, and the selectivity of C_2H_2 decreases from 31 to 11% (Figure 3B). In previous research with the GAP,[34] a constant CO_2/CH_4 ratio of 1 was used, and the focus was on the optimal effective conversion and EC, which were achieved with 20% N_2. However, the CO and H_2 selectivities were almost the lowest at this N_2 fraction, compared with other N_2 fractions. Our results indicate that these selectivities may be enhanced by increasing the CO_2/CH_4 ratio.

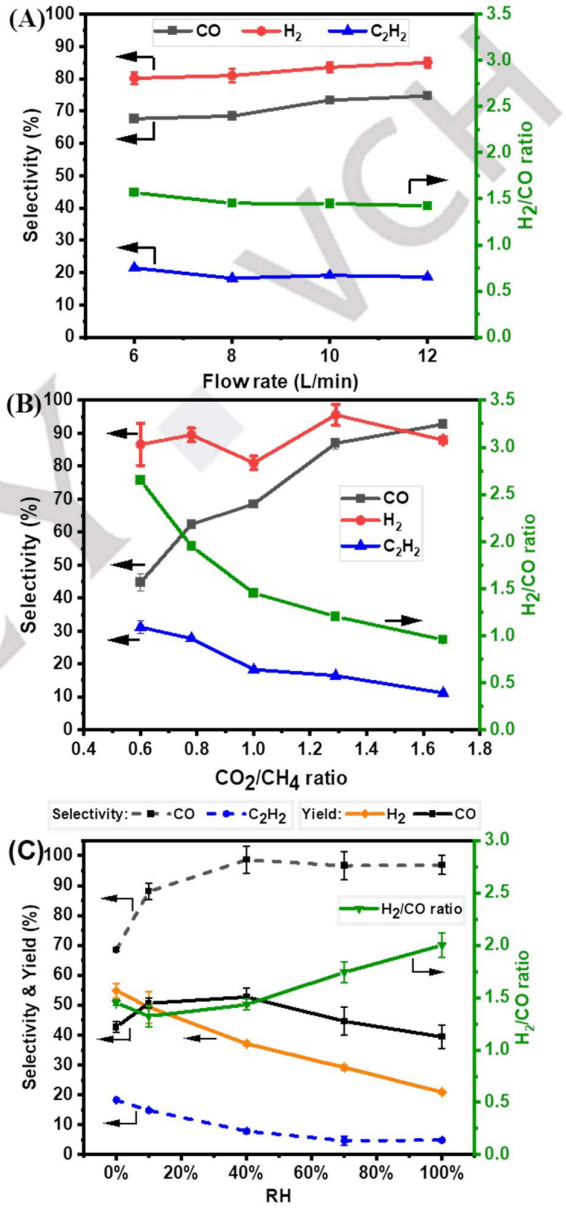

Figure 3. (A, B) Selectivity of CO, H_2, C_2H_2 (left y-axes) and H_2/CO ratio (green curves, right y-axes), and © selectivity of CO and C_2H_2 (dashed lines, left y-axis), yield of H_2 and CO (solid lines, left y-axis) and H_2/CO ratio (right y-axis), as a function of gas flow rate (A), gas composition (B) and RH (C). (A) The total gas flow rate varied from 6 to 12 L/min, $CO_2/CH_4/N_2$ = 1/1/8. (B) Total gas flow rate = 8 L/min, N_2 = 6.4 L/min, CO_2/CH_4 ratio varied between 0.6 and 1.67. (C) Total gas flow rate = 8 L/min, $CO_2/CH_4/N_2$ = 1/1/8, the H_2O amount varied between 0% and 100% RH.

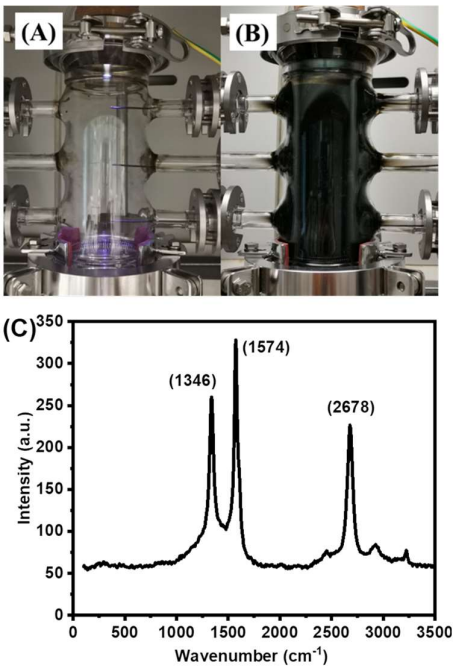

Figure 4. Photographs of post-plasma reactor tube and the Raman spectrum of the solid carbon product collected from the GAP DRM in the (B) case, at a total gas flow rate of 8 L/min, N_2 = 6.4 L/min, for (A) CO_2/CH_4 = 1.67, (B) CO_2/CH_4 = 0.6, (C) Raman spectrum of carbon collected in the (B) case.

Figure 4 compares photographs of the post-plasma reactor tube when using CO_2/CH_4 ratios of 0.6 and 1.67. With higher CO_2 fraction, there was no visible carbon deposition on the inside wall of reactor (Figure 4A), while serious carbon deposition was visible when more CH_4 was added into the feed gas (Figure 4B). We believe this is because the carbon produced from methane ($CH_4 \rightarrow C + 2H_2\ \Delta H^0 = 75.6\,kJ/mol$) reacts directly with CO_2 or with the oxygen atom produced by CO_2, promoting the CO production. Indeed, such reactions were demonstrated to happen also when placing a carbon bed after the GAP plasma reactor, as demonstrated by detailed chemistry modeling.[41] This also explains why the C_2H_2 selectivity decreases, as more C atoms recombine with O atoms to form CO rather than C_2H_2. Raman spectroscopy, as shown in Figure. 4C, was employed to analyze the composition of the carbon on the reactor's inner wall. Distinct carbon signals were detected at around 1346 cm^{-1} (D band) and 1574 cm^{-1} (G band), with an I_D/I_G value of 0.79. The D band appears due to the defects of the product, and the G band reflects the in-plane sp2 carbon vibrations. The value of I_D/I_G is used to evaluate the defects of the product: the larger the value, the smaller the size of the product.[18,42] Additionally, a 2D band at 2678 cm^{-1} was observed, which is typically attributed to the overtone of the D band.[18] Although the conversions of CO_2 and CH_4 change only slightly for different CO_2/CH_4 ratios, relatively more H_2 is produced than CO at lower CO_2/CH_4 ratio, creating a maximum H_2/CO ratio of 2.7. This is interesting for further use of the syngas via Fischer-Tropsch synthesis, for example, to produce methanol, for which the ideal H_2/CO ratio is equal to 2.[43]

The selectivity of CO increases significantly once H_2O was added into the feed gas (Figure 3C), although the conversion decreases (Figure 1D) due to the water-gas shift reaction (WGSR) ($CO + H_2O \rightarrow CO_2 + H_2, \Delta H^0 = -42.1\,kJ/mol$). This can be explained by the higher number of O atoms produced from the H_2O molecules, enhancing the oxidation of carbon-containing species (deposited carbon or hydrocarbon species) into CO. This results in the general increasing trend of CO selectivity. Vice versa, the C_2H_2 selectivity decreases upon H_2O addition. Literature reported that the formation of hydrocarbons was strongly affected by the decomposition of CH_4 into CH_3, CH_2, and CH. The addition of H_2O limited the formation of CH, which was proven by optical emission spectrometry,[39] leading to less C_2H_2 formation. Although the outlet water was collected, it was impossible to precisely estimate how much water participated in the reaction, because part of the water condensed and adhered on the walls of the cooling device. Therefore, it was difficult to calculate the H_2 selectivity in a reliable way in this system and the values will not be used here. Upon increasing RH from 10% to 100%, the yield of H_2 exhibited a decrease, as a lot of the H_2O was not involved in the plasma reaction. However, the relative amount of H_2 produced increased with addition of H_2O. As shown in Figure 3C (green line), the H_2/CO ratio drops at first for 10% RH and then increases with increasing amount of H_2O. This is because at low RH, the CO amount increases more than that of H_2, leading to a slight decrease of the ratio. As the RH further increases, the H_2 amount continues to increase, while the CO amount already reached its maximum at 40% RH.

Specific energy input and energy cost

Figure 5 illustrates the specific energy input (SEI) and energy cost (EC) for the various conditions investigated. When only N_2/CO_2 was used for the plasma reaction, the SEI fluctuated between 1.3 and 1.7 kJ/L (Figure. 5A), suggesting that the changes of the gas composition had only small effect on the value of the SEI, as the current was fixed and the power changed only little with gas composition. Different from the SEI, the EC generally exhibits an increasing tendency. With pure CO_2, the EC is 17.1 kJ/L. This value decreases slightly to 15.1 kJ/L as the fraction of N_2 increases to 20%. It rises however to 36.1 kJ/L at a higher N_2 fraction of 40%, fluctuates around this value up to 60% N_2 and then increases to 48 kJ/L with 80% N_2 used. This is directly correlated to the lower effective CO_2 conversion upon higher N_2 fraction, and is most likely due to the higher fraction of energy used to activate the N_2 molecules rather than CO_2.

When increasing the gas flow rate and keeping the gas ratio of $CO_2/CH_4/N_2$ at 1/1/8 (Figure 5B), the SEI decreases linearly, which is logical, as the SEI is inversely proportional to the gas flow rate (see Supporting Information, Eq. S5). However, the EC fluctuates between 5.6 and 6.2 kJ/L, with a maximum value at a gas flow rate of 6 L/min. As the EC is relatively stable, the gas flow rate seems to have little effect on the energy needed for molecules to be converted. More or less the same can be concluded about the effect of the CO_2/CH_4 ratio, because the SEI and EC steadily decrease only from 3.7 to 3.2 kJ/L and from 6.1 to 5.6 kJ/L, upon increasing the CO_2/CH_4 ratio (Figure 5C). The effect of different N_2 contents on the EC for DRM, at a CO_2/CH_4 ratio of 1, was also studied in,[34] and 20% N_2 addition yielded the lowest EC, in line with our results (Figure 5A). Moreover, the EC can be further slightly reduced by increasing the CO_2/CH_4 ratio, as indicated by our results (Figure 5C).

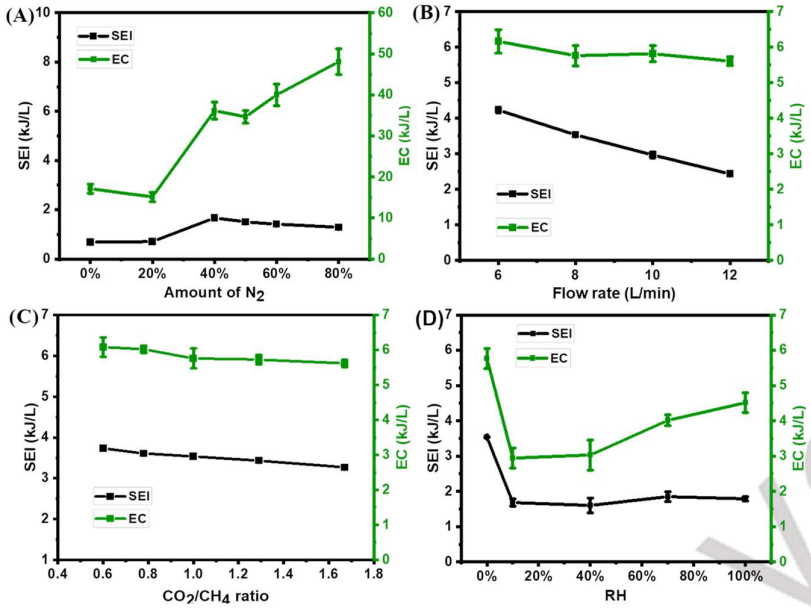

Figure 5. SEI and EC as a function of gas composition, gas flow rate and RH. (A) Total gas flow rate = 10 L/min, N_2 fraction in CO_2 varied from 0% to 80%. (B) The total gas flow rate varied from 6 to 12 L/min, $CO_2/CH_4/N_2$ = 1/1/8. (C) Total gas flow rate = 8 L/min, N_2 = 6.4 L/min, CO_2/CH_4 ratio varied between 0.6 and 1.67. (D) Total gas flow rate = 8 L/min, $CO_2/CH_4/N_2$ = 1/1/8, H_2O amount varied between 0% and 100% RH.

When H_2O is added, the SEI and EC show similar trends (Figure 5D): they decline significantly from 3.5 kJ/L and 5.8 kJ/L to 1.7 kJ/L and 2.9 kJ/L for 10% RH, followed by an increase to 1.9 kJ/L and 4 kJ/L, for 70% RH. Finally, a small decrease in SEI to 1.8 kJ/L but a slightly higher EC of 4.5 kJ/L is observed with 100% RH. Generally, the introduction of H_2O thus results in a lower SEI and EC for the conversion.

Temperature after the plasma

Figure. 6 illustrates the measured post-plasma temperature, at three different distances from the plasma exhaust, for all conditions investigated. All experiments were repeated at least three times, and the detailed temperature data as a function of time, as well as more detailed information, are presented in Figure S3-6. The following conclusions can be drawn from Figure S3-6: (1) The more CO_2 in the N_2/CO_2 system, the more stable is the temperatures measured after plasma, suggesting that CO_2 is beneficial for giving a stable plasma flame. The reason that N_2 addition increases the gas temperature is that the N_2 molecules can acquire energy from the plasma, most of which cannot be used for chemical reaction due to the strong triple bond of N_2, and it can only be vibrationally excited, after which the vibrational levels eventually relax their acquired energy, increasing the gas temperature.[34] (2) Adding CH_4 into the N_2/CO_2 system results in an unstable plasma flame but a generally stable temperature at the same position after plasma. (3) Addition of H_2O (RH ≥ 40%) makes the plasma flame unstable in the first 10 minutes, resulting in a sudden decrease in temperature. This could be due to condensed H_2O inside the cathode, formed during the flushing time.

The temperatures after 10 and 20 minutes of plasma operation at all different conditions are summarized in Figure 6. When N_2 is added into CO_2 (Figure 6A), the temperatures increases at all three distances from the plasma exhaust. As the N_2 fraction increases, the temperature at 4.9 cm increases significantly from 324 °C with pure CO_2 to 569 °C with pure N_2. Although relatively stable in temperature up to 60% N_2, a sharp increase happens when the N_2 concentration is over 60%. Moreover, the temperatures at 10 and 20 minutes are almost the same, suggesting that the temperature was stable after 10 minutes plasma, which was also proven by the data in Figure S3.

Upon adding CH_4 into the CO_2/N_2 mixture and fixing the gas ratio of CO_2/CH_4 to 1 (Figure 6B), the temperature at 4.9 cm first increases upon rising gas flow rate, reaching a maximum value of 516 °C at 10 L/min and then it drops to 481 °C at 12 L/min. However, different from the CO_2/N_2 system, in which the temperature at 9.8 cm and 14.6 cm showed the same trends as at 4.9 cm, the temperature at lower position (9.8 cm) now drops from 417 °C at 8 L/min to 373 °C at 10 L/min, while at 14.6 cm it drops from about 330 °C at 8 L/min to 280 °C at 10 L/min. The lowest temperature at a distance of 9.8 cm and 14.6 cm was measured at a gas flow rate of 10 L/min. The higher temperature might have contributed to the higher conversions of CO_2 and CH_4 as the dry reforming reaction is endothermic. Besides this, as shown in Figure 2B, the cathode melted at 6 L/min, suggesting a higher gas flow rate is necessary.

At fixed gas flow rate, changing the CO_2/CH_4 ratio causes some fluctuation in the temperature at 4.9 cm, in the range between 467 °C and 501 °C after 10 min plasma reaction (Figure 6C). After 20 min, at the same positions, the reactions with higher CO_2 fractions had lower temperature differences with the measurements at 10 min, suggesting that more CO_2 present in the gas flow yields more stable temperatures. This is in accordance with the results in Figure 6A, where higher CO_2 fractions resulted in lower but more stable plasma temperatures.

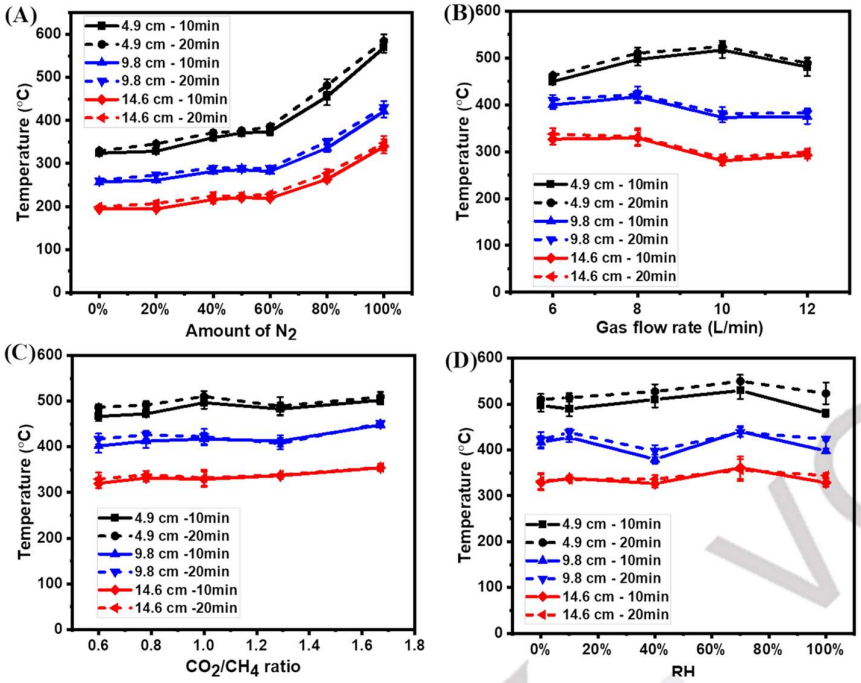

Figure 6. Temperature at 4.9 cm, 9.8 cm, and 14.6 cm after the plasma reactor, for 10 min and 20 min plasma operation, as a function of gas composition, gas flow rate and RH. (A) Total gas flow rate = 10 L/min, N_2 fraction in CO_2 varied from 0% to 100%. (B) The total gas flow rate varied from 6 to 12 L/min, $CO_2/CH_4/N_2$ = 1/1/8. (C) Total gas flow rate = 8 L/min, N_2 = 6.4 L/min, CO_2/CH_4 ratio varied between 0.6 and 1.67. (D) Total gas flow rate = 8 L/min, $CO_2/CH_4/N_2$ = 1/1/8, H_2O amount varied between 0% and 100% RH.

Finally, upon H_2O addition (Figure 6D), the temperature at 4.9 cm first slightly increases and then decreases once the H_2O content is over 70% RH. This could be due to the high heat capacity of H_2O, which adsorbes more heat. At 100% RH, as shown in Figure. S6, the plasma was not stable anymore, leading to lower gas temperatures after the plasma in 10 min. Note that at 9.8 cm, with 40% RH, the temperature dropped from 427 °C to 380 °C (Figure 6D). The reason for this is however unclear.

Computational results and considerations for the post-plasma catalyst bed

Figure. 7 shows the temperature profile in the GAP reactor as calculated by the 3D CFD model. The figure shows that the gas temperature reaches values close to 3500 K in the center of the plasma, which is in line with the calculated gas temperatures for CO_2 and CH_4 plasmas in the GAP from previous work.[32,34] Once the gas reaches the outlet of the reactor, it has cooled down to a gas temperature of around 1100 K. Figure 8A shows the gas temperature profile beyond the GAP reactor in the post-plasma reactor tube, as calculated by the 2D axisymmetric CFD model. This profile shows how the gas cools down further as it leaves the reactor body and flows through the post-plasma reactor tube. From this profile it is clear that the heat of the exhaust gas is not transported evenly over the whole volume of the tube, but is concentrated in the center of the reactor. This is attributed to the high gas flow velocity that is present as the gas flows out through the small reactor outlet, as demonstrated by the calculated gas flow velocity profile in Figure 8B. The high gas flow drags the heat along through convective heat transport, leaving no time for the gas to diffuse in the radial direction through conductive heat transport.

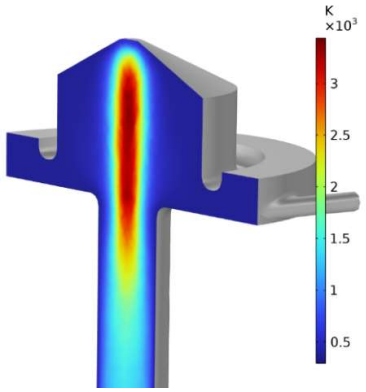

Figure 7. Calculated gas temperature profile in the GAP reactor for a 1/1/8 $CO_2/CH_4/N_2$ gas mixture and a flow rate of 8 L/min.

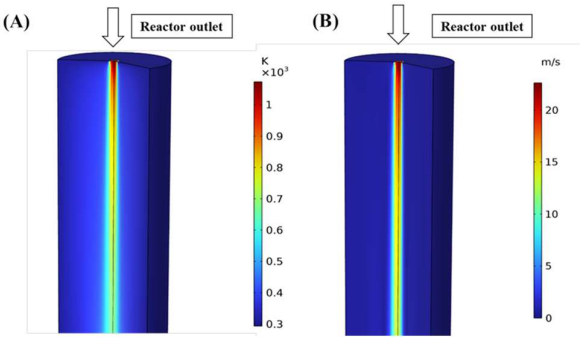

Figure 8. (A) Calculated gas temperature profile and (B) calculated flow velocity profile in the post-plasma reactor tube for a 1/1/8 $CO_2/CH_4/N_2$ mixture gas mixture and a flow rate of 8 L/min.

This has important implications for considering a post-plasma catalyst bed inside the tube, as catalysts located in the center of the tube will experience a significantly higher temperature compared to catalysts near the edge of the tube. As the activity, selectivity and stability of a catalyst are strongly dependent on the temperature, this is an important factor for the post-plasma catalyst process in combination with GAP reactors. For the implementation of a post-plasma catalyst bed, it could thus prove beneficial to disturb the centralized flow stream, by e.g. modifying the reactor outlet with a nozzle, introducing more gas mixing and/or more radial heat transport in the post-plasma tube. Introducing the catalyst bed in the tube will also, to some degree, already introduce some disturbance to the central flow stream. In addition, the experimental results (Figure 6 and Figure S3-S6) show a different temperature depending on the distance of the catalyst bed from the plasma exhaust. It should also be realized that the presence of a catalyst bed will alter the flow behavior and heat transfer,[35] thus necessitating further assessment of the temperature profile once a catalyst bed has been implemented. Nonetheless, our study of the post-plasma zone temperature profile without catalysts has already provided insights into how and where to implement the catalysts, laying a foundation for future studies. Finally, also the feed composition will have an influence on temperature and exhaust gas composition, as demonstrated by the above results and discussion in the temperature part, that can also affect the catalytic performance.

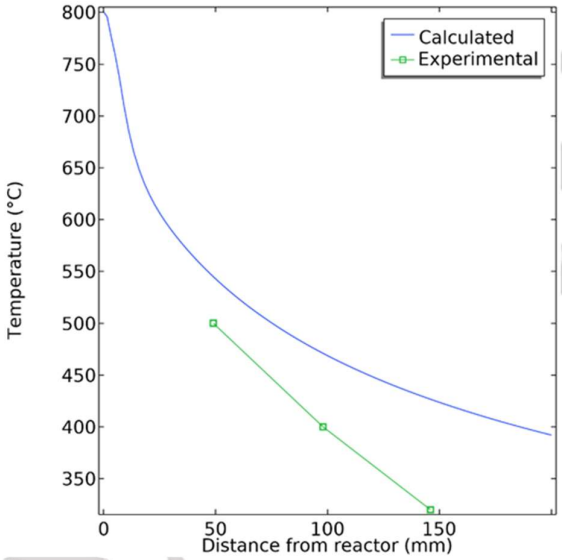

Figure 9. Comparison of temperature measured and modelled for the GAP reactor, as a function of distance from the reactor outlet, at a gas flow rate of 8 L/min and gas composition $CO_2/CH_4/N_2$ = 1/1/8.

Figure 9 displays the axial temperature profile in the center of the post-plasma reactor tube, as calculated by the 2D axisymmetric CFD model, and compared to the thermocouple measurements shown in Figure 6, serving as a validation for the modelling results. While some deviation in absolute values is present and the trend is not the same, a decreasing temperature is observed in both the model and experiments. In general, these results can give us a better idea of where to place a post-plasma catalyst bed. Combined with the experimental results of thermal catalytic DRM,[44–46] which indicated that a temperature above 500 °C is necessary for the catalysts to show catalytic activity, we recommend that the distance of a post-plasma catalyst bed should be shorter than 4.9 cm. Considering the closer the distance from the plasma exhaust, the higher the temperature will be, as well as the possible backflow effect caused by the addition of a catalyst bed,[35] the distance of a post-plasma catalysis bed should be carefully investigated.

Conclusion

We have experimentally investigated the impact of the addition of N_2, N_2/CH_4 (varying gas flow rate and CO_2/CH_4 ratios), and $N_2/CH_4/H_2O$ on the CO_2 (and CH_4) conversion, product selectivity and EC in a GAP. We also measured the temperature at three different distances from the plasma exhaust (4.9 cm, 9.8 cm, and 14.6 cm), and we calculated the temperature distribution inside the GAP and in the post-plasma reactor tube by computational fluid dynamics simulations, to provide insights for potential post-plasma catalyst applications.

Generally, the following conclusions can be drawn:

(1) The addition of N_2 enhances the absolute conversion of CO_2 from 4% without N_2 to 13% with 80% N_2, although the effective conversion decreases due to dilution of CO_2. As a result of the latter, the EC increases significantly upon rising N_2 fraction. Considering that industrial gas emissions contain significant amounts of N_2, a mixture with 80% N_2 content, to achieve high absolute CO_2 conversion, is a reasonable choice, while lower N_2 contents may be more beneficial if the higher EC is the most critical parameter.

(2) The addition of CH_4 in combination with N_2 results in a more complex situation. At fixed CO_2/CH_4 ratio of 1, increasing the gas flow rate from 6 L/min to 12 L/min causes a drop in the CO_2 and CH_4 conversions, selectivity of C_2H_2, ratio of H_2/CO and EC, while the selectivity of CO and H_2 shows an increasing trend. Moreover, the low gas flow rate of 6 L/min damaged the cathode. Increasing the CO_2/CH_4 ratio from 0.6 to 1.67 resulted in an increase in the absolute conversion of CH_4, while the absolute conversion of CO_2 decreased. However, the effective conversion of CH_4 and CO_2 exhibited opposite trends. Besides this, the selectivity of C_2H_2, the H_2/CO ratio, SEI, and EC all decreased with increasing fraction of CO_2. Considering the damage of the GAP device at too low flow rates, and the obtained results for CO_2 and CH_4 conversion, CO and H_2 selectivity, we believe that 8 L/min with $CO_2/CH_4/N_2$ = 1/1/8 is a quite optimal condition.

(3) The addition of H_2O suppressed the conversion of CO_2 and CH_4, with a more pronounced effect on the former, leading to a decrease in the absolute CO_2 conversion from 55% at 0% RH to 22% at 100% RH. However, as the CH_4 conversion was less affected, this improved the H_2/CO ratio from 1.45 to 2. Furthermore, the SEI and EC both decreased significantly when H_2O was added (between 10 and 40% RH) but then increased as the amount of H_2O increased. Thus, H_2O addition can help to improve the H_2 production and decrease the EC, albeit at the expense of some CO_2 conversion, which both help to increase the produced H_2/CO ratio. This is beneficial for the further processing of syngas into other chemicals. However, the amount of H_2O

addition should be carefully studied, as too much H_2O will affect the plasma stability and the post-plasma temperature.

(4) Our measured temperature data suggest that N_2 dilution above 60% will increase the outlet gas temperature. When adding N_2/CH_4 or $N_2/CH_4/H_2O$, no dramatic changes were observed, and the temperatures at three distances from the exhaust generally ranged between 470-520 °C at 4.9 cm, 370-440 °C at 9.8 cm, and 330-350 °C at 14.6 cm. In order to make optimal use of the heat produced by the plasma, for activating post-plasma catalysts, the catalyst bed should thus be placed quite close to the GAP reactor exhaust, dependent on the temperature required for the catalytic process. However, considering the catalyst stability and the effect of active sites sintering at too high temperature, the distance should also not be too close to avoid destroying the catalyst.

(5) Our CFD simulations indicate that the exhaust gas temperature is not transported uniformly over the post-plasma reactor tube but is concentrated in the center. This is also important for considering a post-plasma catalyst bed. Moreover, the simulations confirmed the decreasing temperature with increasing distance from the plasma exhaust.

In summary, our paper provides valuable insights into selecting suitable reaction conditions to achieve higher CO_2 (and CH_4) conversion, lower energy costs, and higher syngas production, also important for post-plasma catalysis, as the exhaust gas of the plasma serves as the feed gas for the post-plasma catalytic reaction. Furthermore, the measured and calculated temperature profiles offer valuable information to design and position a post-plasma catalyst bed, taking the temperature distribution and gradients over the post-plasma reactor tube into account, as well as the impact of gas composition (e.g. dilution) on the post-plasma temperature.

Experimental and computational section

Details on the experimental setup and the computational description, the configurations for plasma reaction, gas products analysis, including how to correct for the gas expansion, the equations defined for conversion, product selectivities, yield, specific energy input and energy cost, and temperature data are provided in the Supporting Information

Supporting Information

The detailed experimental, computational description and temperature data are provided in the Supporting Information.

Acknowledgements

We acknowledge the VLAIO Catalisti Moonshot project D2M and the VLAIO Catalisti transition project CO_2PERATE (HBC.2017.0692) for financial support. We acknowledge Gilles Van Loon for his help to make the quartz and steel devices for the reactor. Vladimir V. Galvita also acknowledges a personal grant from the Research Fund of Ghent University (BOF; 01N16319).

Author Contributions

Wencong Xu performed experiments, data analysis, experimental part writing- original draft and conceptualization. Senne Van Alphen performed computational modelling, computational part writing- original draft and conceptualization. Vladimir V. Galvita performed review, editing, and supervision. Vera Meynen performed writing, review, editing, conceptualization, funding and supervision. Annemie Bogaerts performed writing, review, editing, conceptualization, funding and supervision.

Conflict of interest

The authors declare no conflict of interest.

Keywords: CO_2 conversion • Plasma • Gliding arc plasmatron • Temperature profiles • Computational modelling

[1] F. Van der Ploeg, C. Withageny, *Rev. Environ. Econ. Policy* **2015**, *9*, 285–303.

[2] "National Oceanic and Atmospheric Administration (NOAA) Global Monitoring Laboratory," can be found under https://gml.noaa.gov/ccgg/trends/, **2023**.

[3] J. Ashok, S. Pati, P. Hongmanorom, Z. Tianxi, C. Junmei, S. Kawi, *Catal. Today* **2020**, *356*, 471–489.

[4] G. H. Gunasekar, K. Park, K. D. Jung, S. Yoon, *Inorg. Chem. Front.* **2016**, *3*, 882–895.

[5] M. Liu, Y. Yi, L. Wang, H. Guo, A. Bogaerts, *Catalysts* **2019**, *9*, 275.

[6] M. Pérez-Fortes, J. C. Schöneberger, A. Boulamanti, G. Harrison, E. Tzimas, *Int. J. Hydrogen Energy* **2016**, *41*, 16444–16462.

[7] M. Aresta, A. Dibenedetto, A. Angelini, *Chem. Rev.* **2014**, *114*, 1709–1742.

[8] A. Mustafa, B. G. Lougou, Y. Shuai, Z. Wang, H. Tan, *J. Energy Chem.* **2020**, *49*, 96–123.

[9] S. Saeidi, S. Najari, F. Fazlollahi, M. K. Nikoo, F. Sefidkon, J. J. Klemeš, L. L. Baxter, *Renew. Sustain. Energy Rev.* **2017**, *80*, 1292–1311.

[10] I. V. Yentekakis, P. Panagiotopoulou, G. Artemakis, *Appl. Catal. B Environ.* **2021**, *296*, 120210.

[11] R. Snoeckx, A. Bogaerts, *Chem. Soc. Rev.* **2017**, *46*, 5805–5863.

[12] M. Ramakers, G. Trenchev, S. Heijkers, W. Wang, A. Bogaerts, *ChemSusChem* **2017**, *10*, 2642–2652.

[13] L. Di, J. Zhang, X. Zhang, *Plasma Process. Polym.* **2018**, *15*, e1700234.

[14] G. Chen, R. Snyders, N. Britun, *J. CO2 Util.* **2021**, *49*, 101557.

[15] N. . Anoop, S. Sundaramurthy, J. M. Jha, S. Chandrabalan, N. Singh, J. Verma, D. Parvatalu, S. Katti, *Clean Technol. Environ. Policy* **2021**, *23*, 2789–2811.

[16] R. S. Abiev, D. A. Sladkovskiy, K. V. Semikin, D. Y. Murzin, E. V. Rebrov, *Catalysts* **2020**, *10*, 1358.

[17] E. Suslova, S. Savilov, A. Egorov, A. Shumyantsev, V. Lunin, *Microporous Mesoporous Mater.* **2020**, *293*, 109807.

[18] C. Wang, D. Li, Z. S. Lu, M. Song, W. Xia, *Chem. Eng. Sci.* **2020**, *227*, 115921.

[19] W. C. Chung, M. B. Chang, *Renew. Sustain. Energy Rev.* **2016**, *62*, 13–31.

[20] V. Palma, M. Cortese, S. Renda, C. Ruocco, M. Martino, E. Meloni, *Nanomaterials* **2020**, *10*, 1596.

[21] S. Li, R. Ahmed, Y. Yi, A. Bogaerts, *Catalysts* **2021**, *11*, 590.

[22] R. Aerts, W. Somers, A. Bogaerts, *ChemSusChem* **2015**, *8*, 702–716.

[23] H. Kim, S. Song, C. P. Tom, F. Xie, *J. CO2 Util.* **2020**, *37*, 240–247.

[24] E. Cleiren, S. Heijkers, M. Ramakers, A. Bogaerts, *ChemSusChem* **2017**, *10*, 4025–4036.

[25] T. Kozàk, A. Bogaerts, *Plasma Sources Sci. Technol.* **2014**, *23*, 045004.

[26] J. Feng, X. Sun, Z. Li, X. Hao, M. Fan, P. Ning, K. Li, *Adv. Sci.* **2022**, *9*, 1–36.

[27] G. Trenchev, A. Bogaerts, *J. CO2 Util.* **2020**, *39*, 101152.

[28] Y. Wang, N. Wang, J. Harding, G. Chen, X. Tu, *Plasma Technology for Syngas Production*, Elsevier Inc., **2023**.

[29] H. Sun, Z. Chen, J. Chen, H. Long, Y. Wu, W. Zhou, *J. Phys. D. Appl. Phys.* **2021**, *54*, 495203.

[30] H. Zhang, L. Li, X. Li, W. Wang, J. Yan, X. Tu, *J. CO2 Util.* **2018**, *27*, 472–479.

[31] F. Jardali, S. Van Alphen, J. Creel, H. Ahmadi Eshtehardi, M. Axelsson, R. Ingels, R. Snyders, A. Bogaerts, *Green Chem.* **2021**, *23*, 1748–1757.

[32] G. Trenchev, S. Kolev, W. Wang, M. Ramakers, A. Bogaerts, *J. Phys. Chem. C* **2017**, *121*, 24470–24479.

[33] J. Slaets, M. Aghaei, S. Ceulemans, S. Van Alphen, A. Bogaerts, *Green Chem.* **2020**, *22*, 1366–1377.

[34] S. Van Alphen, J. Slaets, S. Ceulemans, M. Aghaei, R. Snyders, A. Bogaerts, *J. CO2 Util.* **2021**, *54*, 101767.

[35] H. Zhang, L. Li, R. Xu, J. Huang, N. Wang, X. Li, X. Tu, *Waste Dispos. Sustain. Energy* **2020**, *2*, 139–150.

[36] Z. A. Allah, J. C. Whitehead, *Catal. Today* **2015**, *256*, 76–79.

[37] J. L. Liu, Z. Li, J. H. Liu, K. Li, H. Y. Lian, X. S. Li, X. Zhu, A. M. Zhu, *Catal. Today* **2019**, *330*, 54–60.

[38] M. Ramakers, S. Heijkers, T. Tytgat, S. Lenaerts, A. Bogaerts, *J. CO2 Util.* **2019**, *33*, 121–130.

[39] Y. Xia, N. Lu, N. Jiang, K. Shang, Y. Wu, *J. CO2 Util.* **2020**, *37*, 248–259.

[40] R. Snoeckx, A. Ozkan, F. Reniers, A. Bogaerts, *ChemSusChem* **2017**, *10*, 409–424.

[41] F. Girard-Sahun, O. Biondo, G. Trenchev, G. van Rooij, A. Bogaerts, *Chem. Eng. J.* **2022**, *442*, 136268.

[42] J. Ma, X. Chen, M. Song, C. Wang, W. Xia, *Diam. Relat. Mater.* **2021**, *117*, 108445.

[43] Y. J. Liu, N. Cui, P. L. Jia, X. Wang, W. Huang, *ACS Sustain. Chem. Eng.* **2020**, *8*, 6634–6646.

[44] X. Lin, R. Li, M. Lu, C. Chen, D. Li, Y. Zhan, L. Jiang, *Fuel* **2015**, *162*, 271–280.

[45] D. Y. Kalai, K. Stangeland, Y. Jin, Z. Yu, *J. CO2 Util.* **2018**, *25*, 346–355.

[46] Z. Taherian, V. Shahed Gharahshiran, A. Khataee, Y. Orooji, *Fuel* **2022**, *311*, 122620.